Variational Assimilation of Cloud Liquid/Ice Water Path and Its Impact on NWP

YAODENG CHEN,* HONGLI WANG,[+,#] JINZHONG MIN,* XIANG-YU HUANG,[@] PATRICK MINNIS,[&] RUIZHI ZHANG,* JULIE HAGGERTY,[**] AND RABINDRA PALIKONDA[++]

* *Key Laboratory of Meteorological Disaster of Ministry of Education, Nanjing University of Information Science and Technology, Nanjing, China*
[+] *Cooperative Institute for Research in the Atmosphere, Colorado State University, Fort Collins, Colorado*
[#] *Global Systems Division, NOAA/Earth System Research Laboratory, Boulder, Colorado*
[@] *Centre for Climate Research Singapore, Meteorological Service Singapore, Singapore*
[&] *NASA Langley Research Center, Hampton, Virginia*
[**] *National Center for Atmospheric Research,[##] Boulder, Colorado*
[++] *Science Systems and Applications, Inc., Hampton, Virginia*

(Manuscript received 18 September 2014, in final form 17 April 2015)

ABSTRACT

Analysis of the cloud components in numerical weather prediction models using advanced data assimilation techniques has been a prime topic in recent years. In this research, the variational data assimilation (DA) system for the Weather Research and Forecasting (WRF) Model (WRFDA) is further developed to assimilate satellite cloud products that will produce the cloud liquid water and ice water analysis. Observation operators for the cloud liquid water path and cloud ice water path are developed and incorporated into the WRFDA system. The updated system is tested by assimilating cloud liquid water path and cloud ice water path observations from Global Geostationary Gridded Cloud Products at NASA. To assess the impact of cloud liquid/ice water path data assimilation on short-term regional numerical weather prediction (NWP), 3-hourly cycling data assimilation and forecast experiments with and without the use of the cloud liquid/ice water paths are conducted. It is shown that assimilating cloud liquid/ice water paths increases the accuracy of temperature, humidity, and wind analyses at model levels between 300 and 150 hPa after 5 cycles (15 h). It is also shown that assimilating cloud liquid/ice water paths significantly reduces forecast errors in temperature and wind at model levels between 300 and 150 hPa. The precipitation forecast skills are improved as well. One reason that leads to the improved analysis and forecast is that the 3-hourly rapid update cycle carries over the impact of cloud information from the previous cycles spun up by the WRF Model.

1. Introduction

Initialization of the cloud components in numerical models is important because these quantities are the cumulative products of atmospheric moisture and hydrometeor transport plus complicated nonlinear physical processes associated with cloud development and decay (Raymond et al. 1995; Errico et al. 2007; Bauer et al. 2011; Pincus et al. 2011; Kerr et al.2015; Jones and Stensrud 2015). Several cloud analysis systems have been used to create an initial state, including hydrometeors for numerical weather prediction (NWP) models (Albers et al. 1996; Benjamin et al. 2004; Hu et al. 2006a,b; Auligné et al. 2011). However, Auligné et al. (2011) pointed out that "cloud distributions and mixing ratios are retrieved through non-variational adjustments of moisture and/or temperature" in the current cloud analysis systems and "more studies are required to retrieve hydrometeors in balance with the model prognostic variables."

Over the past decade, additional attention has also been paid to directly analyzing cloud components for NWP models using advanced data assimilation techniques.

Denotes Open Access content.

[##] The National Center for Atmospheric Research is sponsored by the National Science Foundation.

Corresponding author address: Dr. Hongli Wang, Global Systems Division, NOAA/Earth System Research Laboratory, 325 Broadway, Boulder, CO 80305.
E-mail: hongli.wang@noaa.gov

DOI: 10.1175/JAMC-D-14-0243.1

Many researchers have worked to initialize model hydrometeors with radar (reflectivity) data using three-/four-dimensional variational (3D/4D-Var) data assimilation and ensemble Kalman filter (EnKF) data assimilation systems. The variational systems used for radar reflectivity assimilation include the Advanced Research and Prediction System 3D-Var (Gao and Stensrud 2012), the high-resolution radar data assimilation system at the Naval Research Laboratory (Zhao and Jin 2008), the variational Doppler radar analysis system (Sun and Crook 1998), and the data assimilation (DA) system for the Weather Research and Forecasting (WRF) Model (WRFDA) 4D-Var system (Wang et al. 2013b; Sun and Wang 2013). Although the 4D-Var and EnKF methods show great potential, these approaches still suffer from unaffordable computer costs for operational NWP. Thus, the 3D-Var is still widely used in research communities and operational centers.

In addition to radar observations, satellite data are another source of observations to initialize cloud condensates for NWP models. There are two different approaches to assimilate satellite data. One approach is the direct assimilation of satellite radiances. Assimilating radiances directly can avoid uncertainties and discrepancies in the retrieval algorithms that differ from satellite to satellite (Derber and Wu 1998). Because of the uncertainty of modeling the hydrometeors in NWP and the inaccuracy of the Radiative Transfer Model (RTM) in simulating the cloudy radiance, it is difficult to assimilate radiances in the presence of clouds. Most NWP centers and researchers concentrate on the assimilation of clear-sky microwave and infrared radiances (e.g., Liu et al. 2012; Xu et al. 2013). Considerable progress in directly assimilating cloudy radiances for initializing hydrometeors has been reported by several research groups (Vukicevic et al. 2004; Pavelin et al. 2008; McNally 2009; Polkinghorne and Vukicevic 2011; Stengel et al. 2013; Kostka et al. 2014; Okamoto et al. 2014; Prates et al. 2014).

The other approach is to use retrieved products. The primary drawback to using retrievals in a data assimilation framework is the associated difficulty in assessing uncertainties inherent in that retrieval. However, in contrast with challenges in the direct radiance assimilation for analyzing hydrometeors (Errico et al. 2007; Auligné et al. 2011; Auligné and Wang 2012), the satellite cloud products (such as cloud liquid water path and cloud ice water path) are in fact usually retrieved from visible and (near) infrared radiances that might be not well simulated in RTM and thus are not directly assimilated in most of the current data assimilation systems (Kostka et al. 2014). Assimilating retrieved cloud products is more resource friendly because the observation operator for assimilating retrievals is simpler than that used for radiance assimilation (Migliorini 2012). Moreover, satellite cloud retrievals can provide a reliable, largely untapped source of information on the cloud and the atmospheric state not generally available from other sources (Weisz et al. 2007; Benedetti and Janisková 2008). Recently, cloud water path retrievals from the Geostationary Operational Environmental Satellite (GOES) have been assimilated using the Data Assimilation Research Testbed (DART) ensemble Kalman filter; a severe weather event case study showed that assimilating cloud water path improved representation of both the magnitude and spatial orientation of precipitation (Jones et al. 2013).

Wang et al. (2013a,b) enhanced the WRFDA system to initialize hydrometeors and presented results from assimilating radar reflectivity. However, radar reflectivity data have limited spatial coverage and contain no information on cloud liquid water, and even data from the cloud radar may be less accurate in high-level cloud ice. The objective of this paper is to further develop WRFDA to assimilate satellite cloud liquid water path and ice water path for initializing cloud liquid water and ice water mixing ratios, and assess the impact of assimilating the cloud products on short-term NWP forecasts.

The structure of this paper is as follows. The cloud products and assimilation methodology are described in section 2. Experimental setup and results are presented in section 3. A summary and discussion are given in the final section.

2. Cloud products and assimilation methodology

a. Global Geostationary Gridded Cloud products

The global cloud products used here are the Global Geostationary Gridded Cloud (G3C) products from the NASA Langley Cloud and Radiation Research Group (Minnis 2007; Minnis et al. 2008). The G3C products include cloud liquid and ice water paths and cloud-top and cloud-base pressure, among others, which are retrieved from up to five geostationary satellites. The cloud properties are retrieved for each cloudy pixel using the techniques described by Minnis et al. (2011a). They are then averaged on a uniform grid of 0.25° latitude by 0.3125° longitude. Both pixel and gridded data are available. The G3C set includes data from the Geostationary Operational Environmental Satellites (GOES-East and GOES-West), and the European Meteorological Satellite (Meteosat) Second Generation, the Chinese Fengyun (*FY-2C*), and the Japanese Multifunctional Transport Satellite (MTSAT) satellites. The products provide coverage at all latitudes equatorward of 60° latitude. The G3C products are sampled to

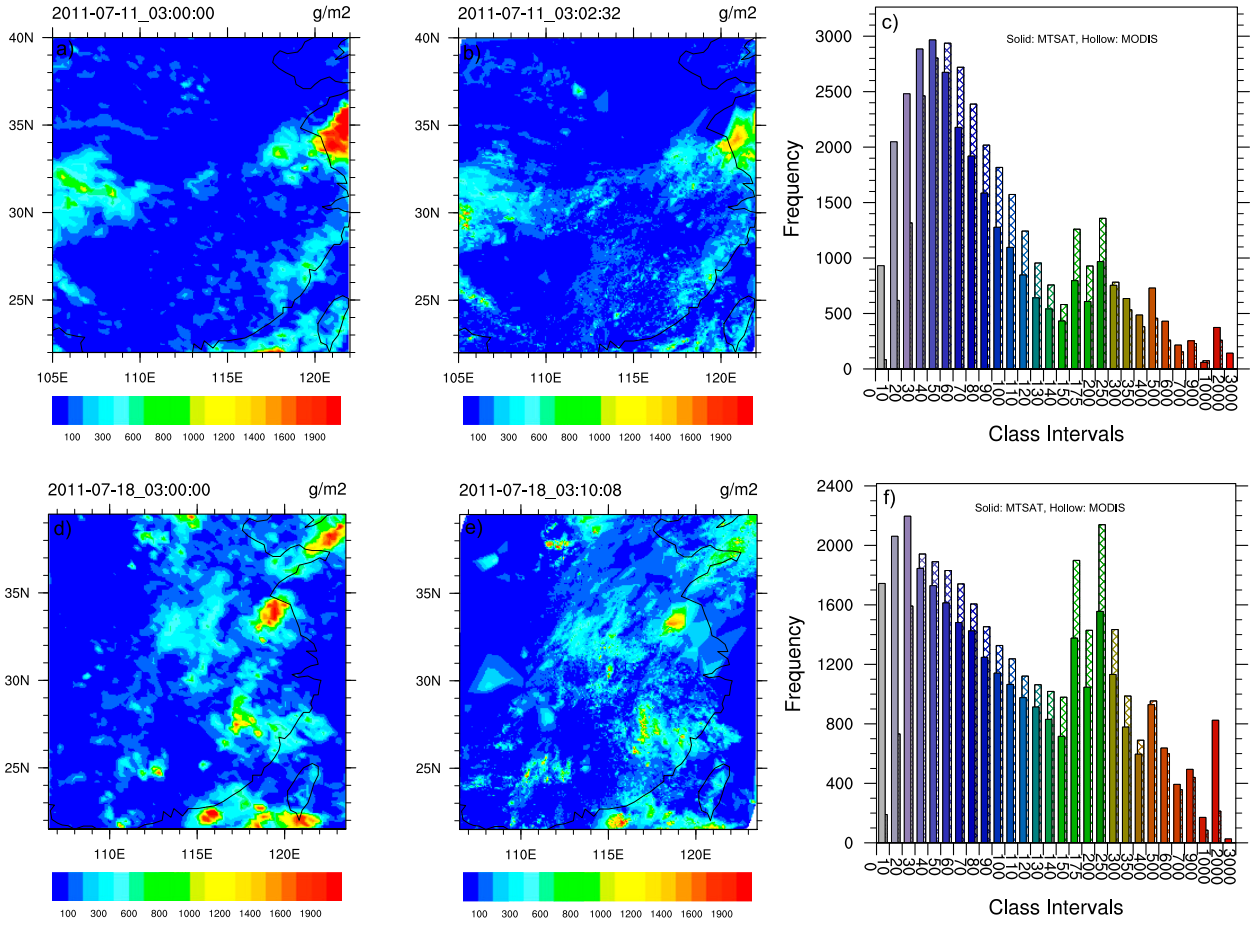

FIG. 1. CWP distribution of (a),(d) G3C and (b),(e) MODIS, and (c),(f) CWP frequency histogram of G3C MTSAT (solid) vs MODIS (hollow). Panels (a)–(c) are at 0300 UTC 11 Jul; (d)–(f) are at 0300 UTC 18 Jul 2011.

achieve a resolution of between 8 and 10 km, depending on the satellite. Full-disk or nearly full-disk data from the satellites are available, at a minimum, each hour from each of the five satellites.

In this study, the cloud ice water path and cloud liquid water path, which represent the amount of cloud water or cloud ice present in an integrated column, are assimilated independently. For simplicity, cloud water path (CWP) is used to represent the ice water path and cloud liquid water path. At a given location, either cloud liquid path or cloud ice water is available. To evaluate the quality of CWP, we compared it with an independent cloud retrieval dataset from the Moderate Resolution Imaging Spectroradiometer (MODIS; Platnick et al. 2003). The MODIS products have high spatial (1 km) resolution but are only available at two local times each day over a given region. Two examples, at 0300 UTC 11 and 18 July 2011, are shown in Fig. 1. The spatial distributions of clouds in G3C are similar to MODIS. The CWP frequency histograms (Figs. 1c, f) show that 1) in the main cloud area (between 40 and 1000 g m^{-2}), the CWP frequency distribution from G3C is close to or less than that from MODIS; and 2) in thin cloud areas (CWP < 40 g m^{-2}) and thick cloud areas (CWP > 2000 g m^{-2}), the frequency distribution of the cloud water path from G3C exceeds that from MODIS. The discrepancies are likely due to viewing angle, resolution, calibration, and retrieval method differences. Although the MODIS products have higher horizontal resolution than their G3C counterparts, the G3C has the merits of greater temporal resolution and global coverage.

b. *Assimilating cloud liquid/ice water path*

The three-dimensional variational component of the WRFDA system (Barker et al. 2012) is used in this study. It is designed to find an analysis that minimizes the following cost function:

$$J(\mathbf{x}) = \frac{1}{2}(\mathbf{x}-\mathbf{x}^b)^{\mathrm{T}}\mathbf{B}^{-1}(\mathbf{x}-\mathbf{x}^b) + \frac{1}{2}[\mathbf{y}-H(\mathbf{x})]^{\mathrm{T}}\mathbf{R}^{-1}[\mathbf{y}-H(\mathbf{x})], \quad (1)$$

where $\mathbf{x}$ is the analysis model vector, $\mathbf{x}^b$ is the background model vector, $\mathbf{y}$ is the observation vector, H is the nonlinear observation operator mapping model space to the observation space, and $\mathbf{B}$ and $\mathbf{R}$ are the background and observation error covariance matrices, respectively.

To assimilate cloud liquid and ice water paths, the observation operators of cloud ice water path and cloud liquid water path, H_{CIP} and H_{CLP}, are defined as

$$H_{\mathrm{CIP}}(\mathbf{q}_i) = \frac{1}{g}\int_{\mathrm{CBP}}^{\mathrm{CTP}} \mathbf{q}_i \, dp \quad \text{and} \tag{2}$$

$$H_{\mathrm{CLP}}(\mathbf{q}_l) = \frac{1}{g}\int_{\mathrm{CBP}}^{\mathrm{CTP}} \mathbf{q}_l \, dp, \tag{3}$$

where CBP and CTP are retrieved cloud-base pressure and cloud-top pressure, respectively. The CBP and CTP are used to constrain the analysis increments inside the cloud regions. The terms $\mathbf{q}_i$ and $\mathbf{q}_l$ represent the cloud ice and cloud water mixing ratios of the atmospheric state, respectively. The cloud control variables are cloud liquid water mixing ratio and cloud ice water mixing ratio.[1]

c. *Observation error specification and cloud product quality control*

The cloud product observation error was estimated using both observation minus background and observation minus analysis information (Desroziers et al. 2005). In the proposed formulation of Desroziers et al. (2005), the observational error variance is the expectation of observation minus background multiplied by observation minus analysis:

$$E[\mathbf{d}_a^o(\mathbf{d}_b^o)^{\mathrm{T}}] = \mathbf{R}. \tag{4}$$

To estimate observational error variances, 6-h WRF forecasts initiated from GFS analyses at 0000 UTC during a 10-day period from 10 to 20 July 2011 were first produced, and then the first guess of the observational error variances was roughly estimated as the variances of the observation minus the 6-h WRF forecasts. Using this first guess of observational error as input to WRFDA, analyses are obtained for calculating observation departure from analyses. With the observation departures from background and analyses, the final estimations of the observational error variance are obtained using Eq. (4). In general, the cloud ice water path error is in the range of 100–500 g m^{-2}, while the cloud liquid water path error is around 50–100 g m^{-2}. In this study, the constants with values of 300 and 60 g m^{-2} are used for cloud ice path and cloud liquid path observations, respectively. Here, it is noted that the errors for the cloud liquid water and ice water are noticeably different. Jones et al. (2013) used a constant value of 50 g m^{-2} CWP error in their EnKF system. The value of 60 g m^{-2} for cloud liquid water path in this research is very close to that value. The observation error values estimated here are also consistent with reports from other studies. It was shown that uncertainties in cloud liquid water path estimated from surface and satellite microwave retrievals are between 30 and 100 g m^{-2} (Dong et al. 2002; Painemal et al. 2012; Xi et al. 2014), and standard deviation of ice water path for global ice cloud mean is about 250 g m^{-2} (Minnis et al. 2011b).

Quality control is an essential step for successfully assimilating the CWP data. To ensure that only good quality data were assimilated, the cloud products underwent the following quality-checking process. First, two quality assurance (QA) flags relevant to cloud liquid/ice water paths provided in the G3C products were used to filter the data. More details on G3C product retrieval algorithm and quality were descripted in Minnis et al. (2011a) and detailed production description can be found online as well (http://cloudsgate2.larc.nasa.gov/). The data were selected while the general QA = 1 and the confidence QA > 1. This ensures that only good and very good products will be assimilated. Second, a maximum check was carried out. The observations with a value greater than 2500 g m^{-2} were discarded. Last, a background check was performed where the observations were rejected if the absolute values of observation departures from background exceeded five times (default value in WRFDA) the observation error.

3. Experimental setup and results

a. *Experimental setup*

Data assimilation cycle and forecast experiments were conducted to assess the impact of the G3C CWP data on short-term regional numerical weather prediction using the Advanced Research WRF Model, version 3.5.1 (V3.5.1). The experiments cover a 10-day period from 10 to 20 July 2011. During this period, sustained rainfall occurred in the Yangtze–Huaihe area and Korean Peninsula. The accumulated precipitation exceeded 100 mm over most of the region. The establishment and maintenance of a blocking system over north China and

[1] Hydrometeor control variables of cloud liquid water mixing ratio, ice water mixing ratio, rainwater mixing ratio and snow water mixing ratio had been developed by Wang et al. (2013a,b). However, only cloud liquid water and rainwater were mentioned in their papers.

the northward movement of a South China Sea low pressure system that brings warm and moist air along a low-level jet are directly related to continuous heavy rain (Liu et al. 2014). The model domain used herein consists of 360 × 240 grid points with 12-km spacing. The physical process schemes were the same as the operational Rapid Update Cycle data assimilation and forecasting system used at the Beijing Meteorological Bureau since 2008 (Wang et al. 2013a). Background error statistics were generated via the National Meteorological Center method (Parrish and Derber 1992) using the utility ''gen_be'' packages in the WRFDA system (Barker et al. 2012).

Two continuous rapid update cycle (3 hourly) assimilation experiments were conducted. The control experiment (EXP-CON) assimilated the National Centers for Environmental Prediction (NCEP) operational Global Telecommunication System (GTS) dataset, which is the same as in Xu et al. (2013). In the second experiment (EXP-CWP), the satellite-derived cloud liquid path and cloud ice path were assimilated along with the GTS observation dataset used in the EXP-CON. We made 24-h forecasts with initial conditions at 0000, 0600, 1200, and 1800 UTC every day.

b. *Verification against GTS observations*

Cloud ice water path accounts for the highest percentage of the observed CWP in the 10-day experiment period. Hence, analysis of cloud ice water mixing ratio in the upper model levels was mostly modified by the CWP assimilation. The modification of cloud liquid and ice water initial conditions can influence the subsequent temperature and humidity forecasts through phase change and interaction with radiation processes and further affect forecasts of other prognostic variables. In this subsection, temperature, humidity, and wind analyses and forecasts at model upper levels were first examined to estimate impact of the CWP assimilation.

Analyses and forecasts are verified against the GTS data. Figures 2a–h show the time series of root-mean-square error (RMSE) of analyses and 12-h forecasts in temperature, u and v wind, and specific humidity at 200 hPa. In the first four cycles (12 h), the differences in RMSE between the two experiments are rather subtle. However, after the fifth cycle, the RMSE of the analyses is noticeably reduced and positive impacts last over the reminder of the data assimilation period (Fig. 2, left column). The positive impact of assimilating CWP can be seen in the 12-h temperature and wind forecasts as well (Fig. 2, right column). The impact of cloud assimilation on 12-h humidity forecasts (Fig. 2d) appears to be neutral. The above results suggest that the assimilation of the cloud products reduces the errors in temperature, humidity, and wind analyses and increases the forecast accuracy of 12-h forecasts of temperatures and wind at 200 hPa. It also found that the surface temperature and humidity analyses are improved (Fig. 3, left column). The analysis error reduction in moisture and temperature, which will provide accurate thermal and instability conditions for convection initiation, is thus expected to lead to improved precipitation skill (Koch et al. 1997; Parsons et al. 2000). The improvements in 12-h surface temperature and humidity forecasts are very slight (Fig. 3, right column).

Figure 4 shows averaged RMSE profiles for temperature, specific humidity, and u and v wind for analyses and forecasts. For temperature, at the upper levels (above 300 hPa), both the analyses and the 12- and 24-h forecasts are improved by assimilating the CWP. For humidity analyses, we see the improvements below 200 hPa as a result of assimilating CWP. However, there is no significant difference between the two experiments in the humidity forecasts.

For the wind analysis and forecasts, it is seen that the RMSE between 100 and 300 hPa in the experiment assimilating cloud liquid/ice water paths is less than that from the control experiment. In addition, the improvement in model upper-level wind forecasts lasts up to 24 h.

c. *Verification against GFS analyses*

To better understand the effects of cloud ice path and cloud liquid water path assimilation, the vertical structures of temperature and humidity analyses and forecasts from the two data assimilations are compared with the final (FNL) global tropospheric analyses produced by the NCEP GFS (http://rda.ucar.edu/datasets/ds083.0/). The GFS final analysis is selected as a reference because the GFS final analyses are accurate enough to describe large-scale systems, since the most complete set of observations including satellite radiances were assimilated to produce the final analysis.

Here we will focus on the thermal and moisture vertical structure comparisons since accurate vertical thermal instability and moisture conditions are crucial for convection initiation and maintenance (Koch et al. 1997; Parsons et al. 2000), especially for summertime heavy rainfall events over Asia (e.g., Zhang and Zhang 2012).

Figure 5 shows the 10-day-averaged south–north section of the averaged temperature difference between EXP-CWP analyses/forecasts and the GFS analyses. A total of 41 analyses and WRF forecasts during the 10 days are used in the calculation. It is seen that the experiment EXP-CON shows a cold bias between the 30th (~388 hPa) and 36th levels (~170 hPa), whereas it shows a warm bias between the 20th (~783 hPa) and

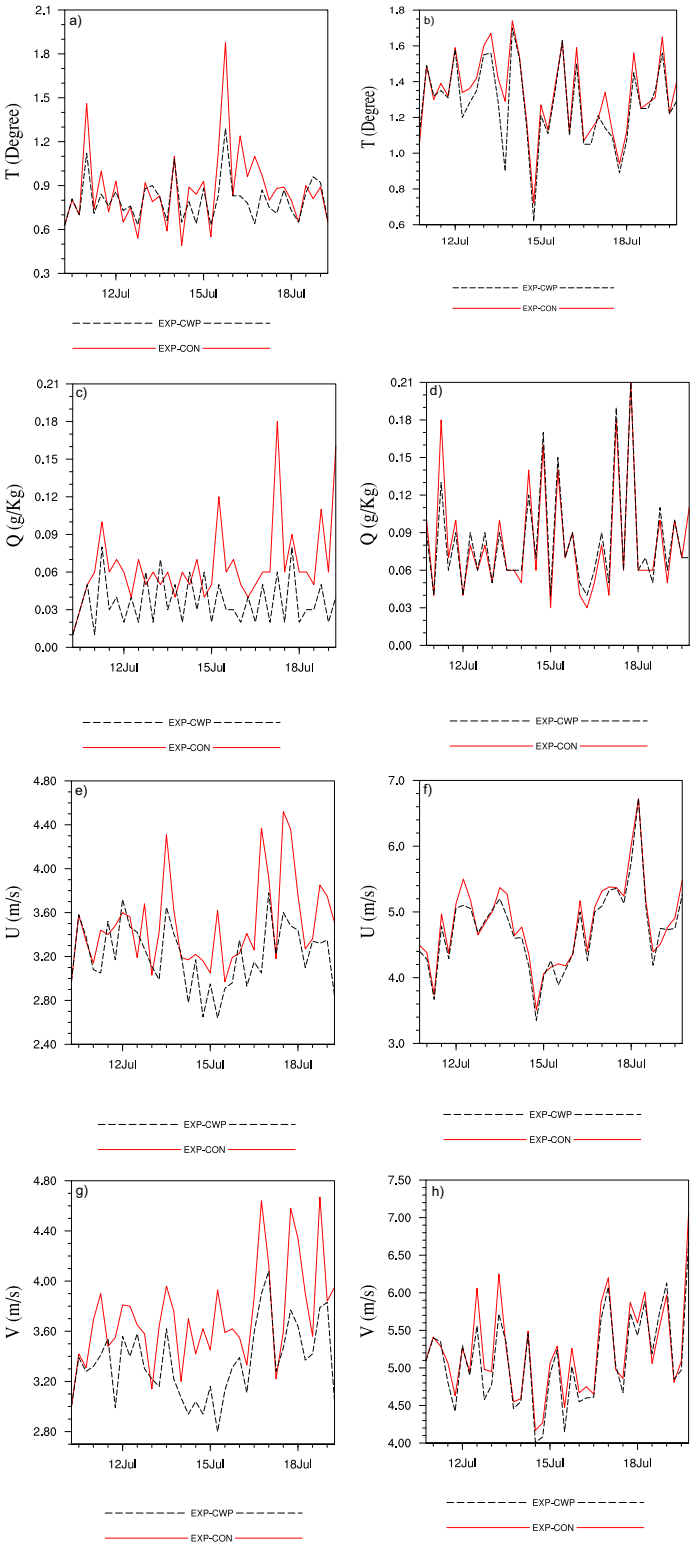

FIG. 2. Time series of RMSE at 200 hPa for (a),(b) temperature; (c),(d) specific humidity; (e),(f) u wind; and (g),(h) v wind for (left) the analyses and (right) the 12-h forecasts.

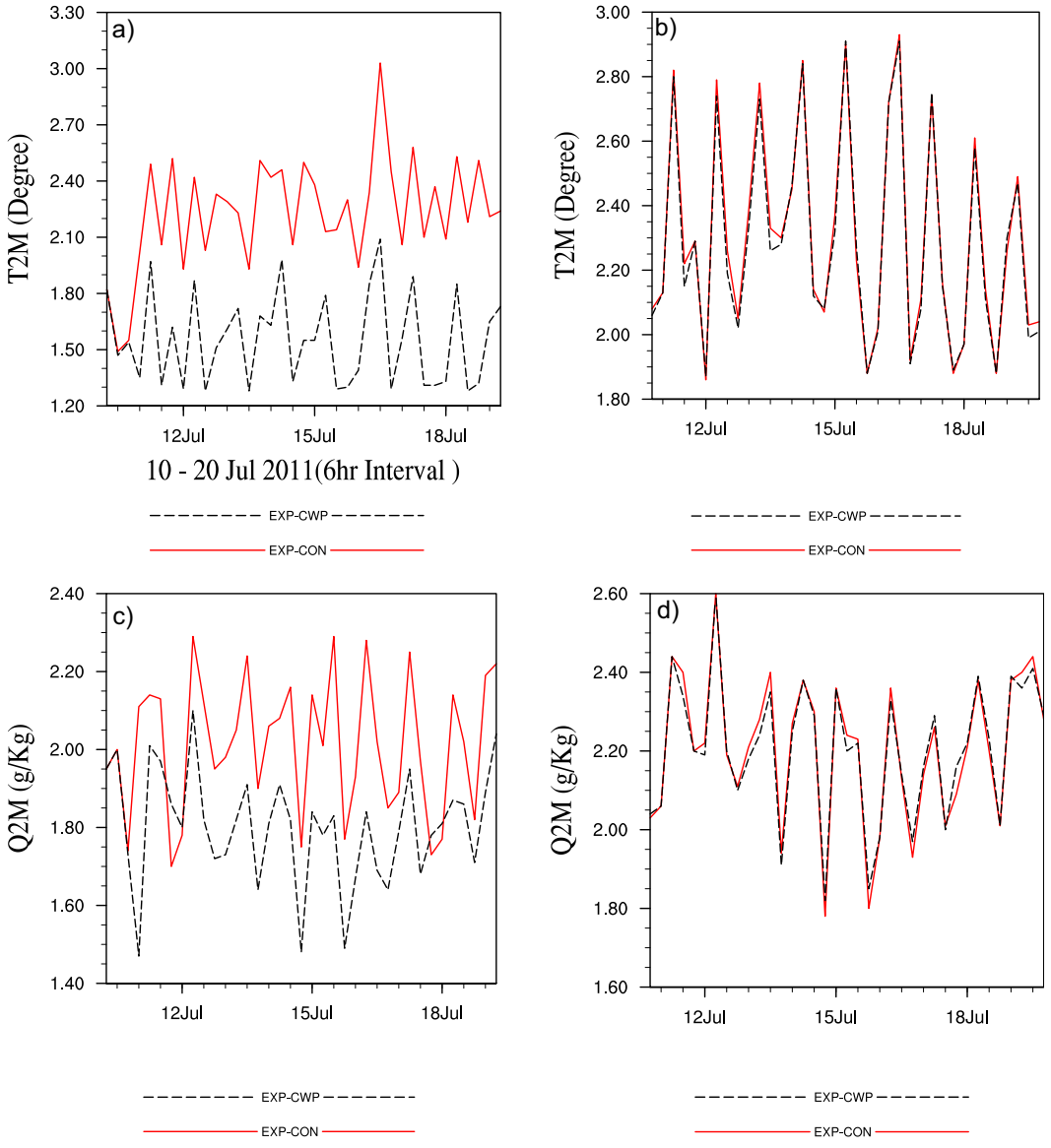

FIG. 3. Time series of RMSE for (a),(b) surface temperature and (c),(d) surface specific humidity for (left) the analyses and (right) the 12-h forecasts.

30th levels (~388 hPa) for both analysis and forecasts. Figure 6 shows the 10-day-averaged south–north section of the averaged temperature difference between the EXP-CWP analyses/forecasts and the EXP-CON analyses/forecasts. In comparing Fig. 5 and Fig. 6, it is seen that EXP-CWP clearly reduces the cold temperature bias close to and above the 30th level (~388 hPa), and it reduces the warm bias between about the 20th (~783 hPa) and 30th levels (~388 hPa). It is noted that the improvement on the temperature field lasts up to 24 h.

As for relative humidity, the experiment EXP-CON shows a dry bias above about the 18th level (~836 hPa) and a wet bias below about the 18th level in both analysis and forecasts (Fig. 7). The dry bias is obviously reduced by assimilating cloud liquid water path and cloud ice water path (Fig. 8). The improvement lasts up to 24 h.

In summary, it is found that assimilation of cloud ice water and liquid water paths greatly reduced the dry moisture bias, the cold temperature bias close to and above 30th level, and the warm bias below the 30th level. These improvements on vertical thermal and moisture fields are beneficial to the maintenance of snow and ice condensates above the mid–upper-level atmosphere and increase vertical thermal instability, which will increase

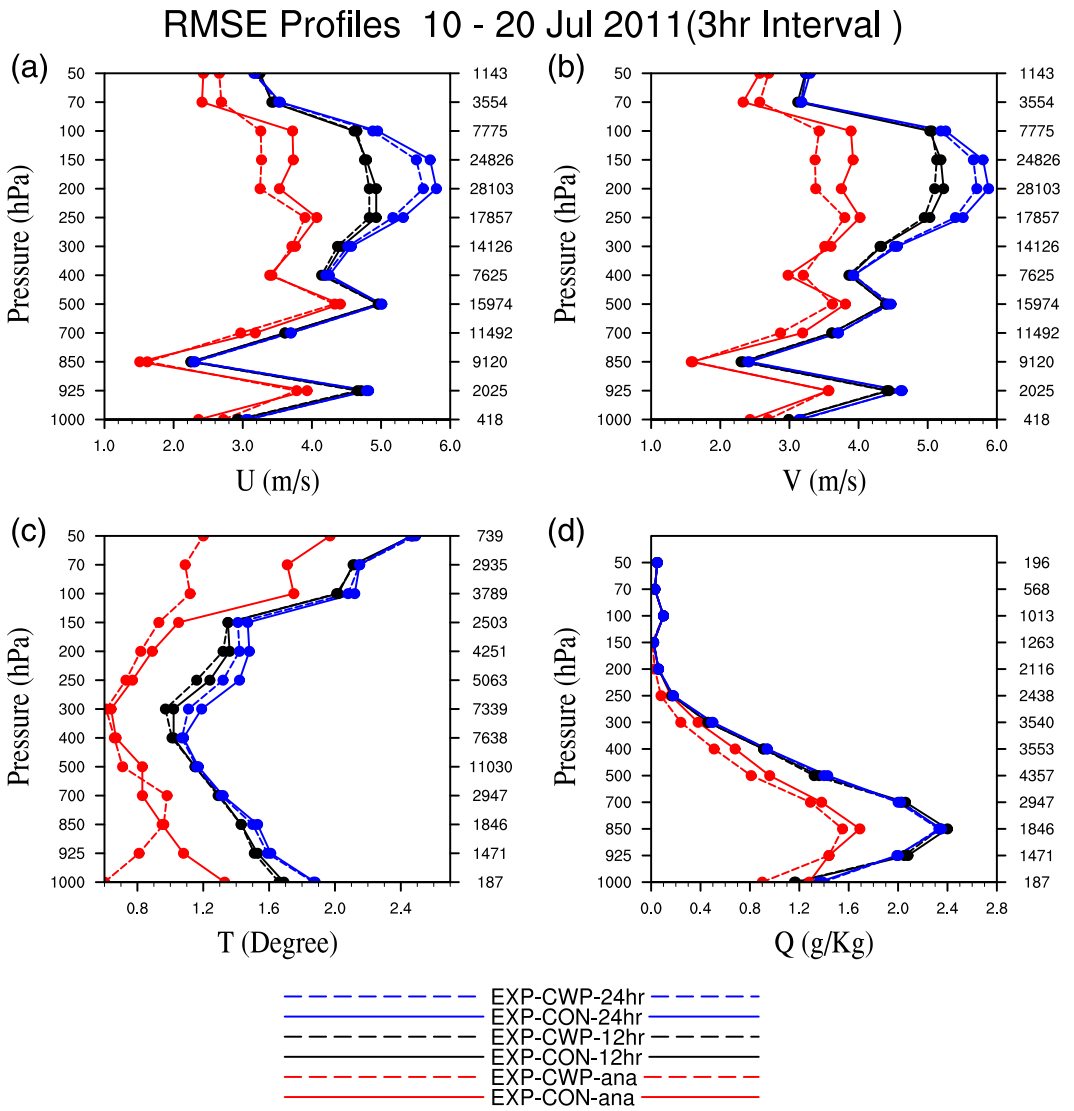

FIG. 4. Averaged vertical RMSE profile for analyses and 12- and 24-h forecasts in comparison with GTS observation: (a) u wind, (b) v wind, (c) temperature, and (d) specific humidity.

cloud and precipitation skill, as will be shown in section 3d.

d. Cloud and precipitation verifications

In the above subsections, it is shown that the most improved regions are in the upper-level atmosphere around 388–170 hPa. Further examination of cloud liquid water path data and cloud ice path data showed that data amount of the cloud ice water path is much greater than the cloud liquid water path, which results in cloud ice increments in upper model levels. Figure 9 shows the south–north section of the averaged ice water mixing ratio difference between EXP-CWP and EXP-CON. It is seen that, for analysis (Fig. 9a), the ice water is increased between the 26th (~550 hPa) and 35th levels (~204 hPa), with a maximum close to the 30th level. For forecasts (Figs. 9b–g), the differences are also mainly in these levels, but the maximum of the differences gradually decreased with forecast time. This is because the cloud liquid/ice water paths retrieved from visible and (near) infrared radiances mainly represent the upper-air cloud water status near the cloud top, whereas the retrievals are based on the visible and (near) infrared radiance. This also explains why the major improvements in the temperature and u and v wind for analyses and forecasts are also between 300 and 150 hPa (Figs. 4, 6, and 8).

Since there is no three-dimensional hydrometeor observation/product over the model domain to directly

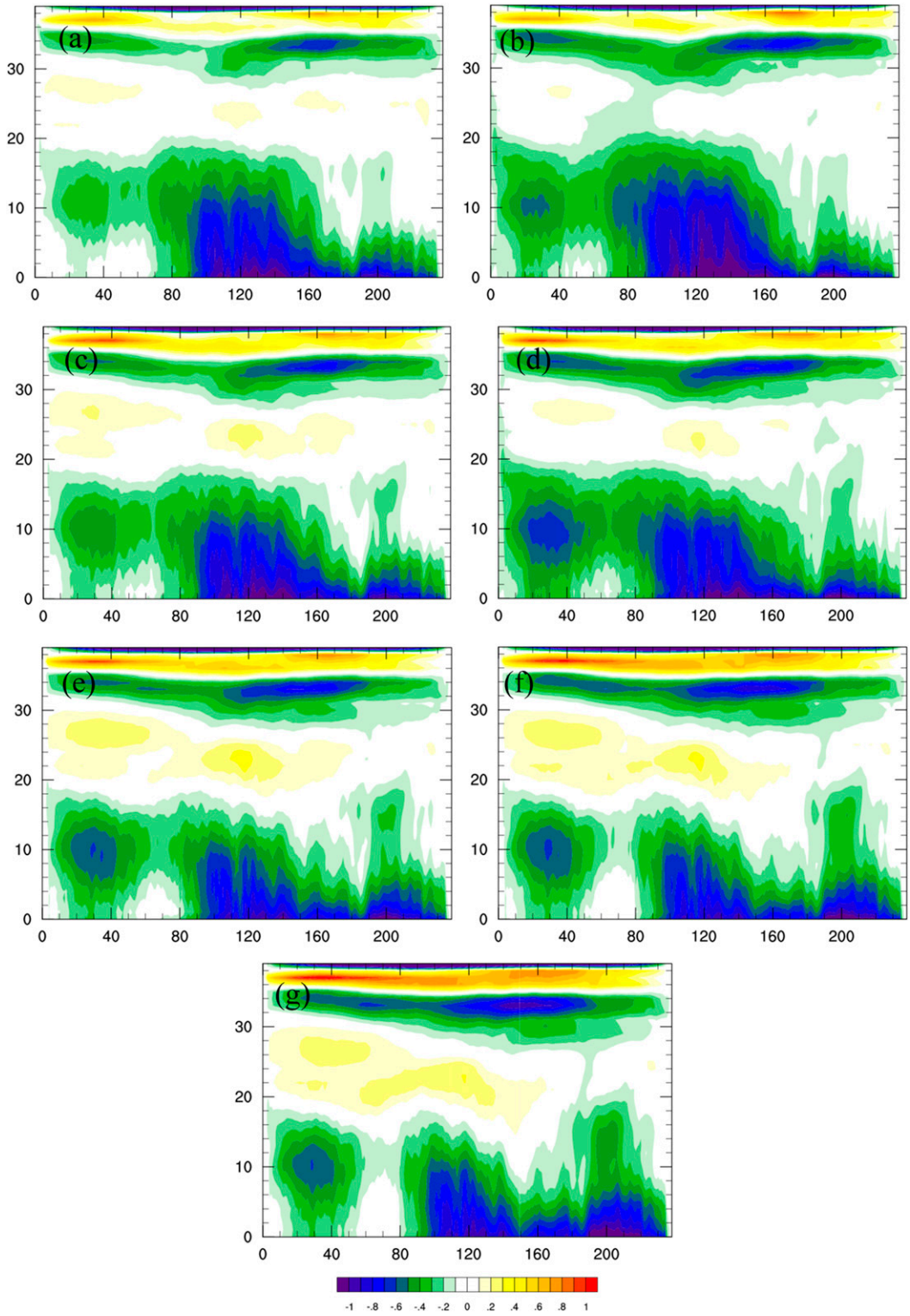

FIG. 5. South–north section of 10-day-averaged temperature difference (°C) between EXP-CON and FNL for (a) analysis and (b) 3, (c) 6, (d) 9, (e) 12, (f) 18, and (g) 24 h.

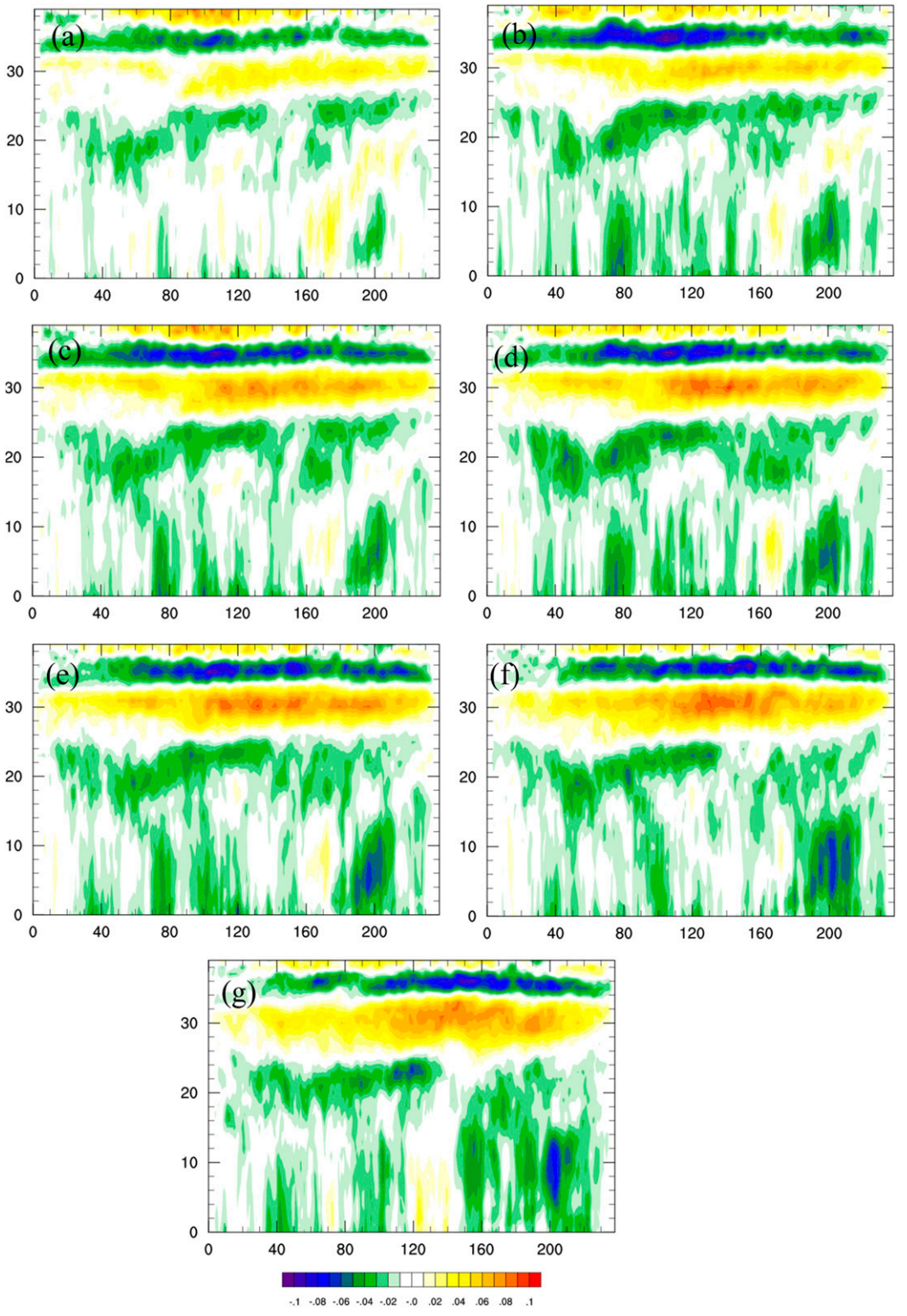

FIG. 6. South–north section of average temperature difference (°C) between EXP-CWP and EXP-CON for (a) analysis and (b) 3, (c) 6, (d) 9, (e) 12, (f) 18, and (g) 24 h.

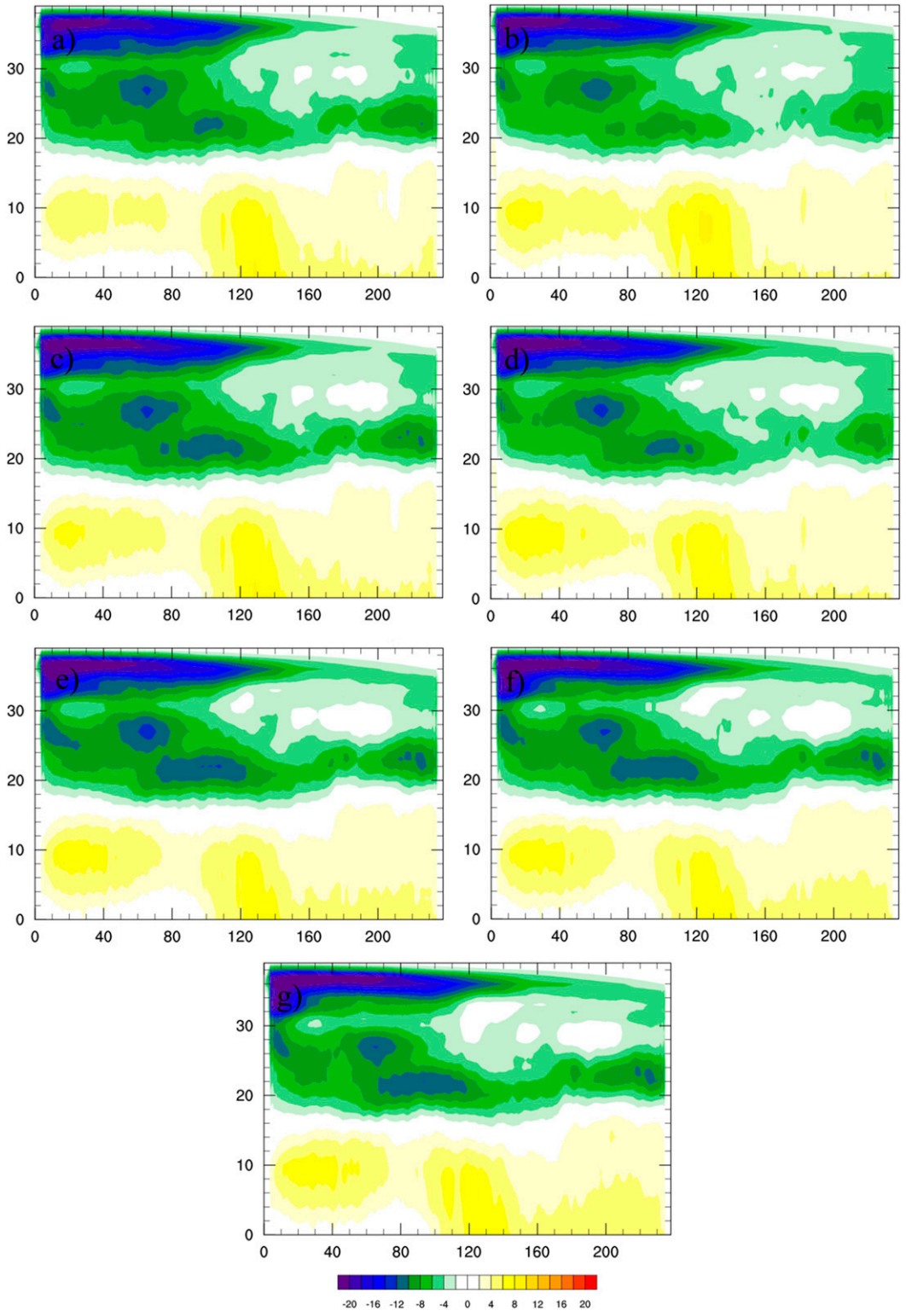

FIG. 7. South–north section of 10-day-averaged relative humidity difference (%) between EXP-CON and FNL for (a) analysis and (b) 3, (c) 6, (d) 9, (e) 12, (f) 18, and (g) 24 h.

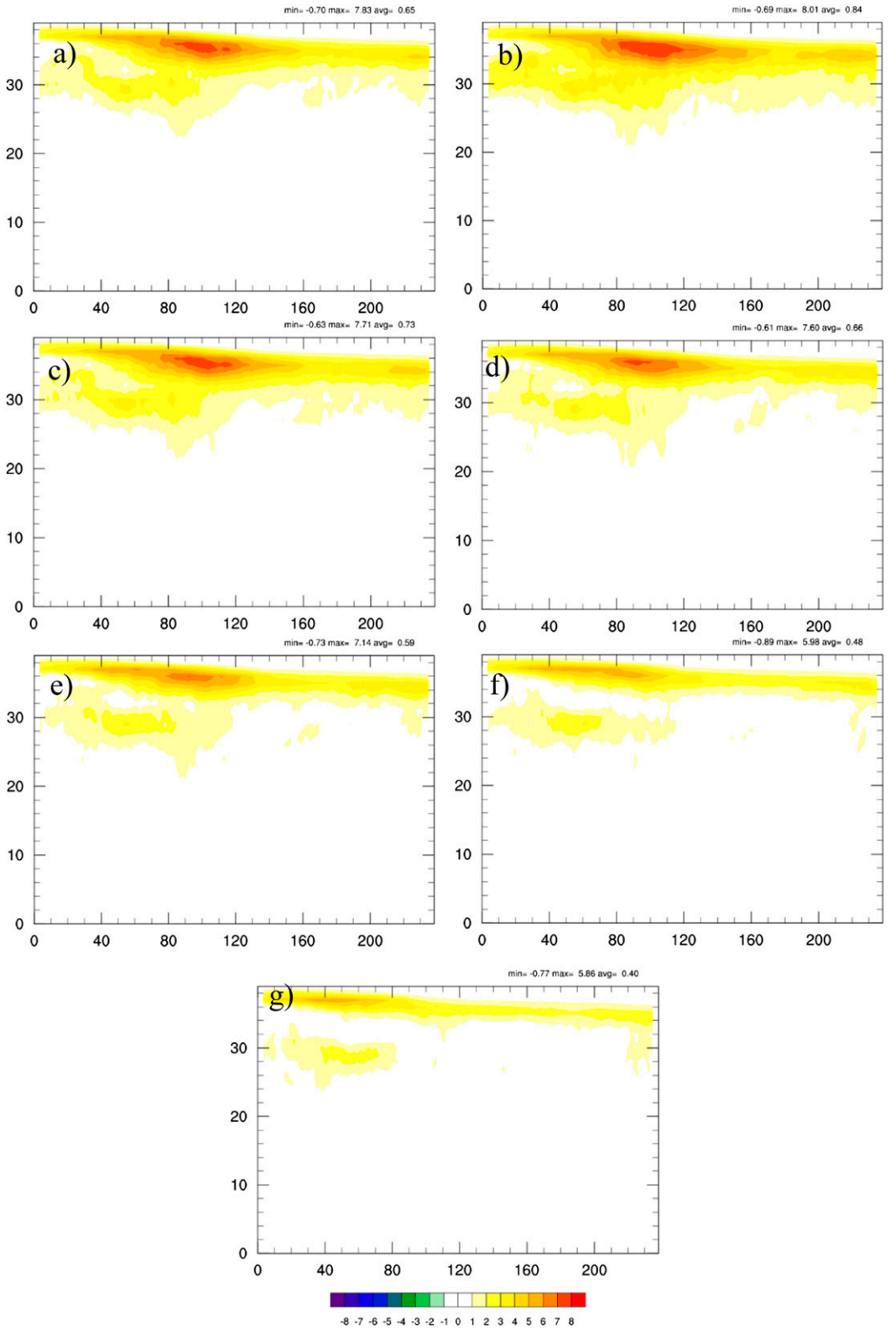

FIG. 8. South–north section of 10-day-averaged relative humidity difference (%) between EXP-CWP and EXP-CON for (a) analysis and (b) 3, (c) 6, (d) 9, (e) 12, (f) 18, and (g) 24 h.

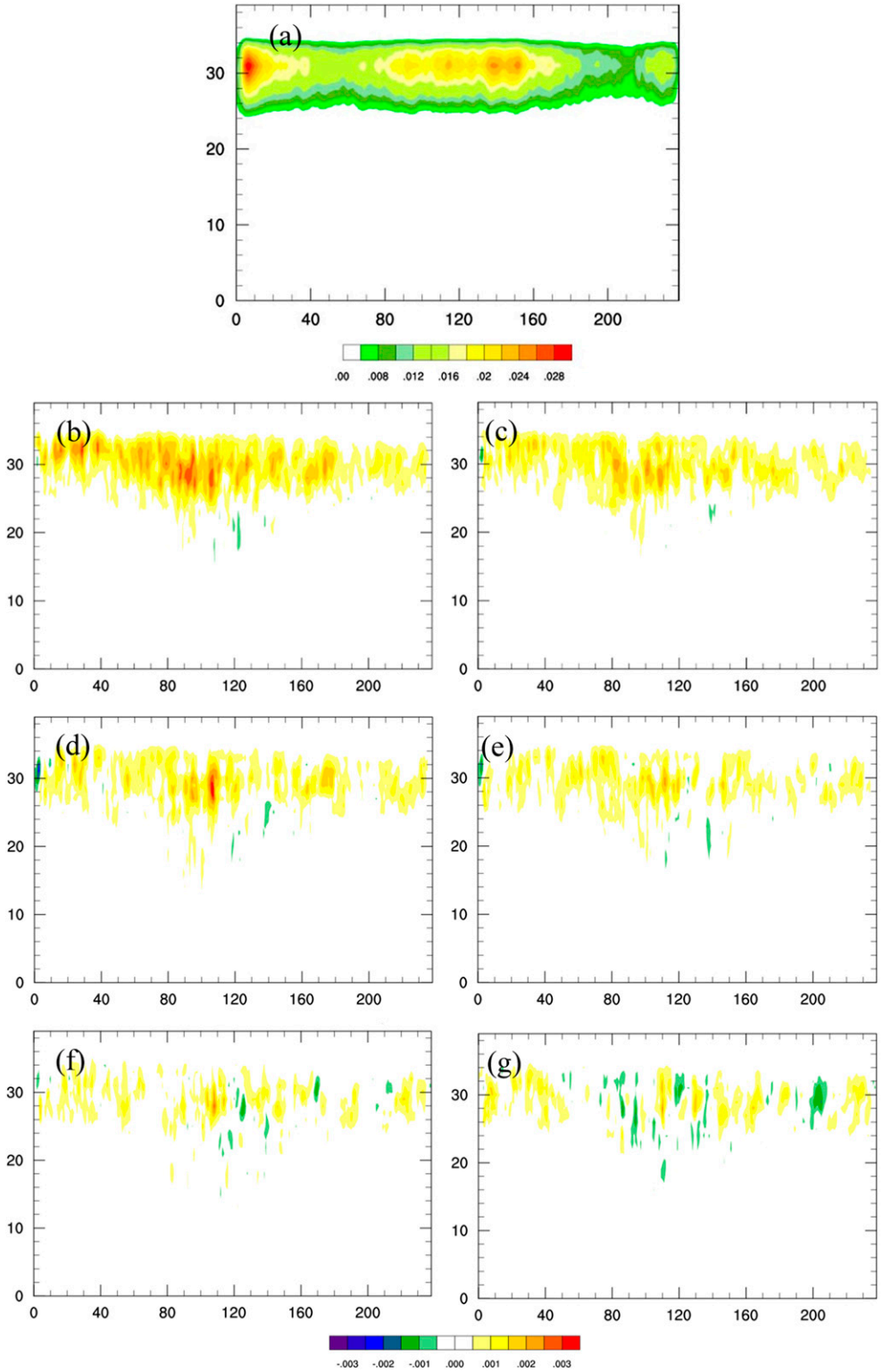

FIG. 9. South–north section of averaged ice water difference (g kg^{-1}) between EXP-CWP and EXP-CON for (a) analysis and (b) 3, (c) 6, (d) 9, (e) 12, (f) 18, and (g) 24 h.

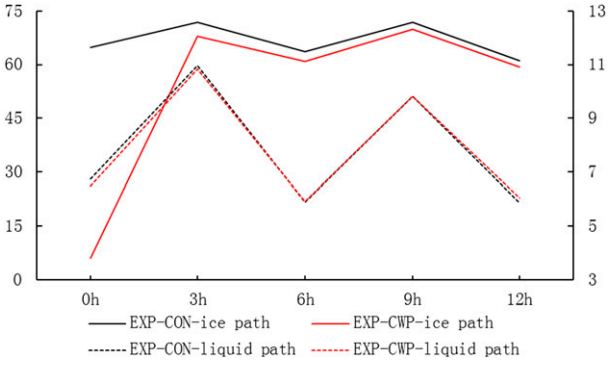

FIG. 10. Biases (g m^{-2}) of cloud ice water path and cloud liquid water path verified against G3C.

verify the hydrometeor analysis, the G3C products are used to verify the WRF cloud fields at analysis and forecast times. Figure 10 shows the biases (absolute values) of WRF-simulated cloud ice water path and cloud liquid water path relative to the G3C products. A total of 41 analyses and WRF forecasts during the 10 days are used to calculate the biases. It is seen that the bias in cloud ice water path at analysis time was significantly reduced in EXP-CWP, and the improvement lasts 12 h. Meanwhile, the impact on the cloud liquid water path is slight because the data amount of cloud liquid water path is less than the cloud ice water path.

The precipitation was verified against the China Hourly Merged Precipitation Analysis (CHMPA), which has an hourly and 0.1° latitude × 0.1° longitude temporal–spatial resolution (Shen et al. 2014). The averaged 24-h accumulated precipitation over the 10-day period from CHMPA and the two experiments are shown in Fig. 11. It can been seen that EXP-CON shows less precipitation than the observations, which indicates the system has a dry bias as shown in the relative humidity analysis (Fig. 7). It is seen that the location and spatial distribution of precipitation forecast by EXP-CWP are much closer to the observations than that from EXP-CON. Additionally, the precipitation intensity forecast near the rainfall center was improved as well.

To provide a quantitative measure of the precipitation forecast skill, the effect of assimilating CWP on precipitation forecasts was assessed using the threat score (TS). Figure 12 shows TS for different precipitation thresholds. Relative to EXP-CON, EXP-CWP noticeably improved the forecast skill of the 6-h accumulated precipitation up to 24 h. Additionally, the positive impacts on TS at large thresholds are more obvious after the 6-h forecasts.

The above results indicate that assimilating cloud products has obvious positive impacts on short-term numerical weather forecasting. One reason that leads to the improved analysis and forecast is that the 3-hourly rapid update cycle carries over the impact of cloud information from the previous cycles spun up by the WRF Model. This is shown in the time series of RMSE in Fig. 2. It is also confirmed by a sensitivity experiment with a 6-hourly cycle that showed less impact of the CWP assimilation (figure not shown).

4. Summary and discussion

This paper aims to further develop WRFDA to assimilate satellite cloud products for initializing cloud liquid water and ice water mixing ratios and assess the effect of assimilating the cloud products on short-term NWP. The updated WRFDA system is tested by assimilating the G3C cloud liquid/ice water path data that

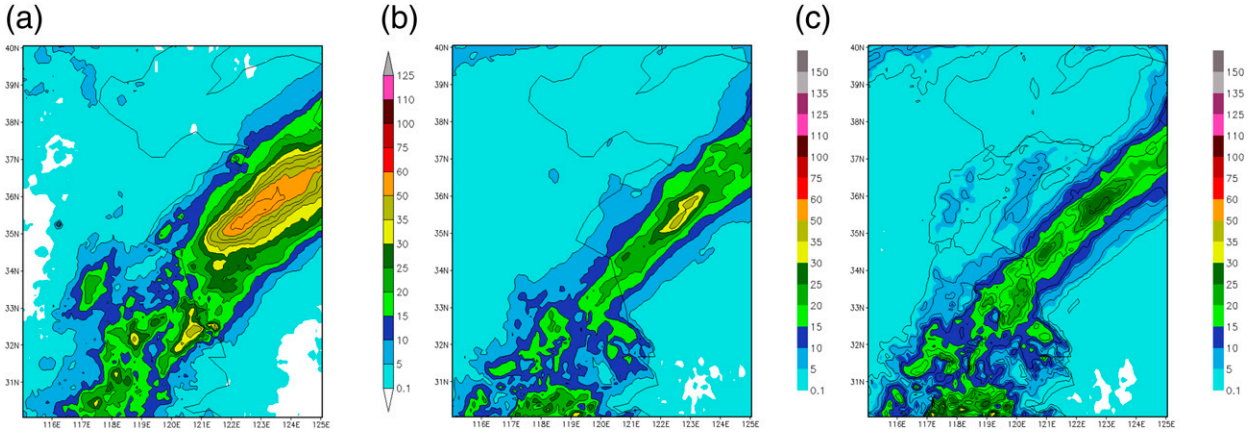

FIG. 11. Averaged 24-h accumulated precipitation: (a) Climate Prediction Center (CPC) morphing technique (CMORPH) precipitation analysis, (b) EXP-CWP, and (c) EXP-CON.

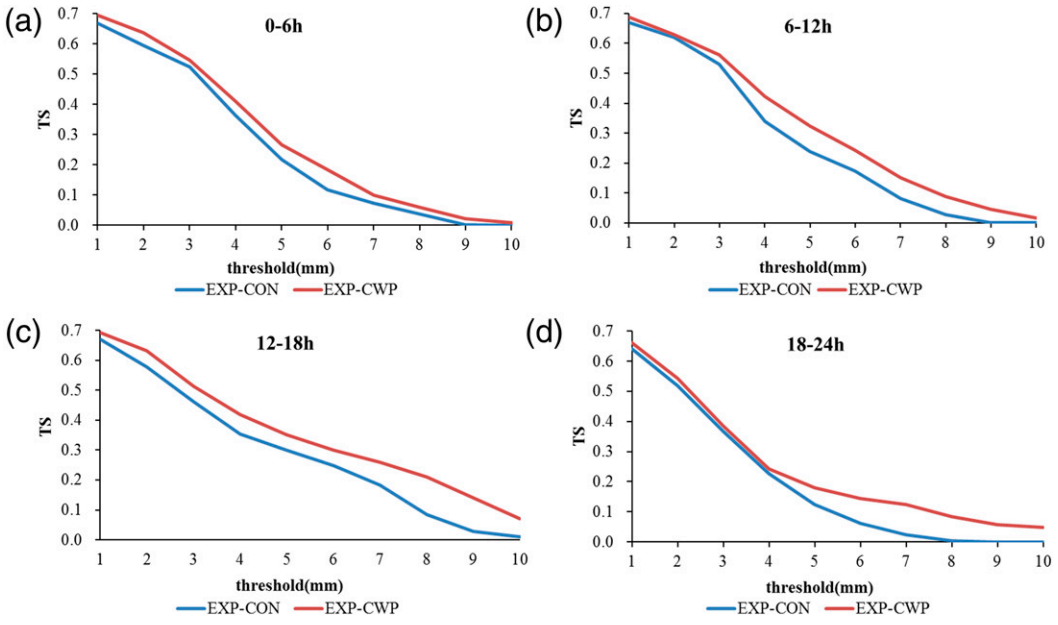

FIG. 12. Threat scores: (a) 0–6-h forecast, (b) 6–12-h forecast, (c) 12–18-h forecast, and (d) 18–24-h forecast.

were retrieved from the visible and (near) infrared geostationary satellite radiances, which are not assimilated in most of current data assimilation systems. Results indicate that assimilating the cloud liquid/ice water path has a positive impact on temperature and wind analysis and forecasts mostly noticeable at high model levels. It is also shown that assimilating cloud liquid/ice water path increases the accuracy of surface temperature and humidity analysis and precipitation forecasts. One reason leading to the improvement in analyses and forecasts is that the 3-hourly rapid update cycle carries over the impact of cloud information from the previous cycles spun-up by the WRF Model.

The cloud liquid/ice water path data assimilation partially mitigates the limitation of the WRFDA cloud analysis that usually depends on observations from the operational weather radar network, which does not observe cloud liquid water and might be less accurate on high-level ice variables. Given the positive results in this study, further research will focus on assimilating both cloud products and radar observations to produce analyses of hydrometeors for WRF. It is expected to be more beneficial to adjust model thermal and dynamical variables through cloud product assimilation by considering background error covariance of cloud condensates and other model variables in a data assimilation system. The multivariate background error covariance will be employed to maximize the impact of the cloud product and radar observations in future studies. This can be achieved by using the WRFDA hybrid variational-ensemble assimilation system (Wang et al. 2008) and/or improving the modeling of the climatological background error covariance (Wang et al. 2014) or the WRFDA 4D-Var system (Wang et al. 2013b; Zhang et al. 2014). Although the above methods may technically provide (flow dependent) multivariate background error covariance that might improve analyses and forecasts, it is of great interest to investigate interactions between microphysics and model dynamics for a deep understanding of cloud data assimilation.

Acknowledgments. This work is jointly sponsored by the 973 Program (2013CB430102), the National Natural Science Foundation of China (41205082), Natural Science Foundation of Jiangsu (BK2012859) and the Priority Academic Program Development of Jiangsu Higher Education Institutions (PAPD). Dr. Minnis and Dr. Palikonda are supported by the NASA Model, Analysis, and Prediction Program. The authors thank Dr. Thomas Auligné, Dr. Yuanfu Xie, and Dr. Zhiquan Liu for discussions on satellite radiance data assimilation. The authors also thank J. C. Osborn at NOAA for providing editorial support for this manuscript.

REFERENCES

Albers, S. C., J. A. McGinley, D. L. Birkenheuer, and J. R. Smart, 1996: The Local Analysis and Prediction System (LAPS): Analyses of clouds, precipitation, and temperature. *Wea. Forecasting,* **11,** 273–287, doi:10.1175/1520-0434(1996)011<0273:TLAAPS>2.0.CO;2.

Auligné, T., and H. Wang, 2012: Assimilation of cloud-affected infrared satellite radiances. Abstract, *13th WRF Users'*

Workshop, Boulder, CO, UCAR, P13. [Available online at http://www2.mmm.ucar.edu/wrf/users/workshops/WS2012/abstracts/p13.htm.]

——, A. Lorenc, Y. Michel, T. Montmerle, A. Jones, M. Hu, and J. Dudhia, 2011: Toward a new cloud analysis and prediction system. *Bull. Amer. Meteor. Soc.,* **92,** 207–210, doi:10.1175/2010BAMS2978.1.

Barker, D., and Coauthors, 2012: The Weather Research and Forecasting Model's Community Variational/Ensemble Data Assimilation System: WRFDA. *Bull. Amer. Meteor. Soc.,* **93,** 831–843, doi:10.1175/BAMS-D-11-00167.1.

Bauer, P., and Coauthors, 2011: Satellite cloud and precipitation assimilation at operational NWP centres. *Quart. J. Roy. Meteor. Soc.,* **137,** 1934–1951, doi:10.1002/qj.905.

Benedetti, A., and M. Janisková, 2008: Assimilation of MODIS cloud optical depths in the ECMWF model. *Mon. Wea. Rev.,* **136,** 1727–1746, doi:10.1175/2007MWR2240.1.

Benjamin, S. G., and Coauthors, 2004: An hourly assimilation-forecast cycle: The RUC. *Mon. Wea. Rev.,* **132,** 495–518, doi:10.1175/1520-0493(2004)132<0495:AHACTR>2.0.CO;2.

Derber, J. C., and W.-S. Wu, 1998: The use of TOVS cloud-cleared radiances in the NCEP SSI analysis system. *Mon. Wea. Rev.,* **126,** 2287–2299, doi:10.1175/1520-0493(1998)126<2287:TUOTCC>2.0.CO;2.

Desroziers, G., L. Berre, B. Chapnik, and P. Poli, 2005: Diagnosis of observation, background and analysis-error statistics in observation space. *Quart. J. Roy. Meteor. Soc.,* **131,** 3385–3396, doi:10.1256/qj.05.108.

Dong, X., P. Minnis, G. G. Mace, W. L. Smith Jr., M. Poellot, R. T. Marchand, and A. D. Rapp, 2002: Comparison of stratus cloud properties deduced from surface, GOES, and aircraft data during the March 2000 ARM Cloud IOP. *J. Atmos. Sci.,* **59,** 3265–3284, doi:10.1175/1520-0469(2002)059<3265:COSCPD>2.0.CO;2.

Errico, R. M., P. Bauer, and J.-F. Mahfouf, 2007: Issues regarding the assimilation of cloud and precipitation data. *J. Atmos. Sci.,* **64,** 3785–3798, doi:10.1175/2006JAS2044.1.

Gao, J., and D. J. Stensrud, 2012: Assimilation of reflectivity data in a convective-scale, cycled 3DVAR framework with hydrometeor classification. *J. Atmos. Sci.,* **69,** 1054–1065, doi:10.1175/JAS-D-11-0162.1.

Hu, M., M. Xue, and K. Brewster, 2006a: 3DVAR and cloud analysis with WSR-88D level-II data for the prediction of the Fort Worth, Texas, tornadic thunderstorms. Part I: Cloud analysis and its impact. *Mon. Wea. Rev.,* **134,** 675–698, doi:10.1175/MWR3092.1.

——, ——, J. Gao, and K. Brewster, 2006b: 3DVAR and cloud analysis with WSR-88D level-II data for the prediction of the Fort Worth, Texas, tornadic thunderstorms. Part II: Impact of radial velocity analysis via 3DVAR. *Mon. Wea. Rev.,* **134,** 699–721, doi:10.1175/MWR3093.1.

Jones, T. A., and D. J. Stensrud, 2015: Assimilating cloud water path as a function of model cloud microphysics in an idealized simulation. *Mon. Wea. Rev.,* **143,** 2052–2081, doi:10.1175/MWR-D-14-00266.1.

——, ——, P. Minnis, and R. Palikonda, 2013: Evaluation of a forward operator to assimilate cloud water path into WRF-DART. *Mon. Wea. Rev.,* **141,** 2272–2289, doi:10.1175/MWR-D-12-00238.1.

Kerr, C. A., D. J. Stensrud, and X. Wang, 2015: Assimilation of cloud top temperature and radar observations of an idealized splitting supercell using an Observing System Simulation Experiment. *Mon. Wea. Rev.,* **143,** 1018–1034, doi:10.1175/MWR-D-14-00146.1.

Koch, S. E., A. Aksakal, and J. T. McQueen, 1997: The influence of mesoscale humidity and evapotranspiration fields on a model forecast of a cold-frontal squall line. *Mon. Wea. Rev.,* **125,** 384–409, doi:10.1175/1520-0493(1997)125<0384:TIOMHA>2.0.CO;2.

Kostka, P. M., M. Weissmann, R. Buras, B. Mayer, and O. Stiller, 2014: Observation operator for visible and near-infrared satellite reflectances. *J. Atmos. Oceanic Technol.,* **31,** 1216–1233, doi:10.1175/JTECH-D-13-00116.1.

Liu, M., J. W. Yu, G. R. Han, and P.-B. Zhang, 2014: Analysis of circulation feature of a continuous heavy rain in Yangtze-Huaihe basin during mid-July in 2011. *J. Trop. Meteor.,* **30,** 153–160.

Liu, Z., C. S. Schwartz, C. Snyder, and S. Y. Ha, 2012: Impact of assimilating AMSU-A radiances on forecasts of 2008 Atlantic tropical cyclones initialized with a limited-area ensemble Kalman filter. *Mon. Wea. Rev.,* **140,** 4017–4034, doi:10.1175/MWR-D-12-00083.1.

McNally, A. P., 2009: The direct assimilation of cloud affected satellite infrared radiances in the ECMWF 4D-Var. *Quart. J. Roy. Meteor. Soc.,* **135,** 1214–1229, doi:10.1002/qj.426.

Migliorini, S., 2012: On the equivalence between radiance and retrieval assimilation. *Mon. Wea. Rev.,* **140,** 258–265, doi:10.1175/MWR-D-10-05047.1.

Minnis, P., 2007: Cloud retrievals from GOES-R. *Proc. OSA Hyperspectral Imaging and Sounding of the Environment Topical Meeting,* Santa Fe, NM, Optical Society of America, HWC3m, doi:10.1364/HISE.2007.HWC3.

——, and Coauthors, 2008: Near-real time cloud retrievals from operational and research meteorological satellites. *Remote Sensing of Clouds and the Atmosphere XIII,* R. H. Picard et al., Eds., International Society for Optical Engineering (SPIE Proceedings, Vol. 7107), doi:10.1117/12.800344.

——, and Coauthors, 2011a: CERES Edition-2 cloud property retrievals using TRMM VIRS and *Terra* and *Aqua* MODIS data—Part I: Algorithms. *IEEE Trans. Geosci. Remote Sens.,* **49,** 4374–4400, doi:10.1109/TGRS.2011.2144601.

——, and Coauthors, 2011b: CERES Edition-2 cloud property retrievals using TRMM VIRS and *Terra* and *Aqua* MODIS data—Part II: Examples of average results and comparisons with other data. *IEEE Trans. Geosci. Remote Sens.,* **49,** 4401–4430, doi:10.1109/TGRS.2011.2144602.

Okamoto, K., A. P. McNally, and W. Bell, 2014: Progress towards the assimilation of all-sky infrared radiances: An evaluation of cloud effects. *Quart. J. Roy. Meteor. Soc.,* **140,** 1603–1614, doi:10.1002/qj.2242.

Painemal, D., P. Minnis, J. K. Ayers, and L. O'Neill, 2012: *GOES-10* microphysical retrievals in marine warm clouds: Multi-instrument validation and daytime cycle over the southeast Pacific. *J. Geophys. Res.,* **117,** D19212, doi:10.1029/2012JD017822.

Parrish, D. F., and J. C. Derber, 1992: The National Meteorological Center's spectral statistical-interpolation analysis system. *Mon. Wea. Rev.,* **120,** 1747–1763, doi:10.1175/1520-0493(1992)120<1747:TNMCSS>2.0.CO;2.

Parsons, D. B., M. A. Shapiro, and E. Miller, 2000: The mesoscale structure of a nocturnal dryline and of a frontal–dryline merger. *Mon. Wea. Rev.,* **128,** 3824–3838, doi:10.1175/1520-0493(2001)129<3824:TMSOAN>2.0.CO;2.

Pavelin, E., S. English, and J. Eyre, 2008: The assimilation of cloud-affected infrared satellite radiances for numerical weather prediction. *Quart. J. Roy. Meteor. Soc.,* **134,** 737–749, doi:10.1002/qj.243.

Pincus, R., R. J. Patrick Hofmann, J. L. Anderson, K. Raeder, N. Collins, and J. S. Whitaker, 2011: Can fully accounting for clouds in data assimilation improve short-term forecasts by global models? *Mon. Wea. Rev.,* **139,** 946–957, doi:10.1175/2010MWR3412.1.

Platnick, S., M. D. King, S. A. Ackerman, W. P. Menzel, B. A. Baum, J. C. Riedl, and R. A. Frey, 2003: The MODIS cloud products: Algorithms and examples from *Terra*. *IEEE Trans. Geosci. Remote Sens.,* **41,** 459–473, doi:10.1109/TGRS.2002.808301.

Polkinghorne, R., and T. Vukicevic, 2011: Data assimilation of cloud-affected radiances in a cloud-resolving model. *Mon. Wea. Rev.,* **139,** 755–773, doi:10.1175/2010MWR3360.1.

Prates, C., S. Migliorini, S. English, and E. Pavelin, 2014: Assimilation of satellite infrared sounding measurements in the presence of heterogeneous cloud fields. *Quart. J. Roy Meteor. Soc.,* **140,** 2062–2077, doi:10.1002/qj.2279.

Raymond, W. H., W. S. Olson, and G. Callan, 1995: Diabatic forcing and initialization with assimilation of cloud water and rainwater in a forecast model. *Mon. Wea. Rev.,* **123,** 366–382, doi:10.1175/1520-0493(1995)123<0366:DFAIWA>2.0.CO;2.

Shen, Y., P. Zhao, Y. Pan, and J. Yu, 2014: A high spatiotemporal gauge satellite merged precipitation analysis over China. *J. Geophys. Res. Atmos.,* **119,** 3063–3075, doi:10.1002/2013JD020686.

Stengel, M., M. Lindskog, P. Undén, and N. Gustafsson, 2013: The impact of cloud-affected IR radiances on forecast accuracy of a limited-area NWP model. *Quart. J. Roy. Meteor. Soc.,* **139,** 2081–2096, doi:10.1002/qj.2102.

Sun, J., and N. A. Crook, 1998: Dynamical and microphysical retrieval from Doppler radar observations using a cloud model and its adjoint. Part II: Retrieval experiments of an observed Florida convective storm. *J. Atmos. Sci.,* **55,** 835–852, doi:10.1175/1520-0469(1998)055<0835:DAMRFD>2.0.CO;2.

——, and H. Wang, 2013: Radar data assimilation with WRF 4D-Var: Part II. Comparison with 3D-Var for a squall line over the U.S. Great Plains. *Mon. Wea. Rev.,* **141,** 2245–2264, doi:10.1175/MWR-D-12-00169.1.

Vukicevic, T., T. Greenwald, M. Zupanski, D. Zupanski, T. Vonder Haar, and A. Jones, 2004: Mesoscale cloud state estimation from visible and infrared satellite radiances. *Mon. Wea. Rev.,* **132,** 3066–3077, doi:10.1175/MWR2837.1.

Wang, H., J. Sun, S. Fan, and X.-Y. Huang, 2013a: Indirect assimilation of radar reflectivity with WRF 3D-Var and its impact on prediction of four summertime convective events. *J. Appl. Meteor. Climatol.,* **52,** 889–902, doi:10.1175/JAMC-D-12-0120.1.

——, ——, X. Zhang, X.-Y. Huang, and T. Auligné, 2013b: Radar data assimilation with WRF 4D-Var. Part I: System development and preliminary testing. *Mon. Wea. Rev.,* **141,** 2224–2244, doi:10.1175/MWR-D-12-00168.1.

——, X.-Y. Huang, J. Sun, D. Xu, M. Zhang, S. Fan, and J. Zhong, 2014: Inhomogeneous background error modeling for WRF-Var using the NMC method. *J. Appl. Meteor. Climatol.,* **53,** 2287–2309, doi:10.1175/JAMC-D-13-0281.1.

Wang, X., D. M. Barker, C. Snyder, and T. M. Hamill, 2008: A hybrid ETKF–3DVAR data assimilation scheme for the WRF Model. Part I: Observing system simulation experiment. *Mon. Wea. Rev.,* **136,** 5116–5131, doi:10.1175/2008MWR2444.1.

Weisz, E., J. Li, J. Li, D. K. Zhou, H. L. Huang, M. D. Goldberg, and P. Yang, 2007: Cloudy sounding and cloud top height retrieval from AIRS alone single field of view radiance measurements. *Geophys. Res. Lett.,* **34,** L12802, doi:10.1029/2007GL030219.

Xi, B., X. Dong, P. Minnis, and S. Sun-Mack, 2014: Validation of CERES-MODIS Edition 4 marine boundary layer cloud properties using DOE ARM AMF measurements at the Azores. *J. Geophys. Res. Atmos.,* **119,** 9509–9529, doi:10.1002/2014JD021813.

Xu, D., Z. Liu, X.-Y. Huang, J. Min, and H. Wang, 2013: Impact of assimilating IASI radiance observations on forecasts of two tropical cyclones. *Meteor. Atmos. Phys.,* **122,** 1–18, doi:10.1007/s00703-013-0276-2.

Zhang, M., and D.-L. Zhang, 2012: Subkilometer simulation of a torrential-rain-producing mesoscale convective system in east China. Part I: Model verification and convective organization. *Mon. Wea. Rev.,* **140,** 184–201, doi:10.1175/MWR-D-11-00029.1.

Zhang, X., X.-Y. Huang, J. Liu, J. Poterjoy, Y. Weng, F. Zhang, and H. Wang, 2014: Development of an efficient regional four-dimensional variational data assimilation system for WRF. *J. Atmos. Oceanic Technol.,* **31,** 2777–2794, doi:10.1175/JTECH-D-13-00076.1.

Zhao, Q., and Y. Jin, 2008: High-resolution radar data assimilation for Hurricane Isabel (2003) at landfall. *Bull. Amer. Meteor. Soc.,* **89,** 1355–1372, doi:10.1175/2008BAMS2562.1.